Magnetization processes in sputtered FeSiB thin films

Marco Coïsson, Carlo Appino, Federica Celegato, Alessandro Magni, Paola Tiberto, and Franco Vinai
INRIM, Electromagnetism Division, Strada delle Cacce 91, I-10135 Torino, Italy

(Received 25 February 2008; revised manuscript received 17 April 2008; published 3 June 2008)

Magnetic thin films have been obtained by rf sputtering on Si_3N_4 substrates from a $Fe_{78}B_{13}Si_9$ target. The samples, with thickness t of 80 and 305 nm, are partially amorphous; crystalline fraction increases on increasing t. Magnetic force microscopy and magneto-optical images, performed at the remanence on both samples, indicate that for $t=80$ nm the average magnetization lies in the film plane, while for the largest thickness, it is oriented perpendicular to it. Static hysteresis loops have been measured at room temperature by means of a vectorial vibrating sample magnetometer with an auto-rotating head. In this way, two linearly independent components of the magnetization vector can be simultaneously acquired as a function of magnetic field either in the in-plane or out-of-plane configuration, at different angles with respect to a reference direction. In this work, the role of sample shape and magnetic anisotropy has been investigated by paying particular attention to the anhysteretic magnetization process and by considering the two-dimensional behavior of the magnetization vector. The negligible role of the in-plane shape anisotropy has been demonstrated in the specimen displaying out-of-plane anisotropy, whereas the effect of the local demagnetizing fields has been put in evidence in the sample with in-plane anisotropy.

DOI: 10.1103/PhysRevB.77.214404 PACS number(s): 75.30.Gw, 75.50.Kj, 75.70.Kw

I. INTRODUCTION

It is well known that the magnetic anisotropy remains one of the key properties for various applications since the advent of magnetism. In this frame, ultrathin films and multilayers exhibiting a magnetization easy axis oriented either perpendicular or parallel to the surface have in the last decades attracted much interest due to their potential advantages in high-density data storage devices and sensors.[1] As a consequence, the understanding of magnetic phenomena, i.e., magnetization process, in such systems still remains an issue to be addressed for fundamental science as well as for potential applications. The existence of a preferential magnetization direction is determined by the combined effects of all the magnetic anisotropies present. These anisotropies are generally classified as intrinsic, having their origin in the shape, surface or interface of the sample, and extrinsic, having a crystalline origin. A better understanding of the magnetization processes in such systems can be achieved by studying the magnetic domain structure, which gives fundamental information on magnetization and anisotropy distributions. Indeed, the magnetic domain pattern on the sample surface is a key parameter in thin-films research in addition to magnetization process (i.e., a hysteresis loop in both the in-plane and out-of-plane directions). In the case of weak perpendicular anisotropy, the out of the plane anisotropy is not high enough to overcome the shape anisotropy and consequently, the magnetization lies mainly within the plane of the film, giving rise to a peculiar domain structure.[2] In fact, a perpendicular component of the magnetization exists and periodically oscillates with a consequent reduction of the magnetostatic energy of the sample, giving rise to the stripe domains.

Generally, in ferromagnetic materials, the variation of the average magnetization $\vec{M}$ involves two kinds of processes: coherent and/or incoherent rotations of the local magnetization $\vec{M}_i$; and domain wall (DW) assisted magnetization reversals (nucleation of domains and DW displacement). All these phenomena but nucleation can be reversible or irreversible, and in general, act together, and show an intricate interplay. Consequently, the magnetization process, as a whole, is endowed with an intrinsic vector nature and a general theory is still lacking.[3] Nevertheless, the main line of research about the materials' magnetic properties, both from the theoretical and experimental viewpoint, is chiefly focused on their scalar properties. This approach, although able to obtain remarkable results, thanks to the large simplification of the physics problem, neglects some fundamental aspects of the magnetization properties. In literature, experimental results are often represented by a set of measurements monitoring the scalar behavior along different directions, whereas the validation of vector models calls for a more complete investigation.[4–8] In this framework, a model has been recently proposed that is able to describe two-dimensional anhysteretic magnetization processes in amorphous samples, with in-plane uniaxial-induced anisotropy.[9–11] In this work, we extend this vector model to FeSiB amorphous thin films produced by sputtering and having different thicknesses. These samples are characterized by either an uniaxial out-of plane or in plane magnetic anisotropy, in order to get information on the details of the magnetization processes ruling out the role of the various terms of magnetic anisotropy. The proposed theoretical approach will be summarized and expanded in Sec. III, and applied in Sec. IV, where we will also demonstrate that it is valid beyond the framework adopted in its native formulation.

II. EXPERIMENT

FeSiB thin films have been obtained by rf sputtering on Si_3N_4 substrates from a $Fe_{78}B_{13}Si_9$ target. The chamber base pressure was $\approx 1.5 \cdot 10^{-7}$ mbar and the Ar pressure was $\approx 1 \cdot 10^{-2}$ mbar; the rf power was kept at 50 W. Samples have been produced with a thickness t of 305 nm (film n7)

and 80 nm (film n8). X-ray diffraction patterns reveal that the samples are amorphous, with a volume crystalline fraction that increases with increasing thickness and never exceeds ≈32% on thicker samples. Additional details are given in Ref. 12.

Approximately square samples of $\approx 3 \times 3$ mm^2 have been cut from uniformly sputtered substrates. Magnetic domains have been observed with a high resolution magneto-optical Kerr effect system (MOKE) and with a magnetic force microscope (MFM). The magnetooptical measurements were performed with a modified[13–16] high-resolution microscope (Zeiss Axioscop 2 Plus), which was set up to perform measurements in Kerr longitudinal mode. The incident light is *s*-polarized. The microscope uses a Zeiss Axiocam HRm camera (14 bit, Peltier cooled), exploring the domain structure evolution under varying applied field. The time interval between successive frames is in the range 0.6–0.7 s. The field was applied with a pair of Helmholtz coils, which allow the application of fields of up to ≈20 kA/m along the light incidence plane. The observations were made under a sinusoidally varying field, in the frequency interval 1–10 mHz, depending on how steep the hysteresis loop was: very sharp magnetization reversals require lower frequencies to be able to detect domain walls spanning the sample. The enlargement used was 200× (numerical aperture=0.40) in the case of the 305 nm thick film, and 100× (numerical aperture =0.25) in the case of the 80 nm thick film. The domains were investigated along two perpendicular directions to detect the possible presence of anisotropies. Furthermore, the demagnetized state was recorded, in order to understand the equilibrium state of the samples. Although the films' remanence is rather high, we were able to demagnetize all the samples. Prior to acquisition, a reference state is captured at saturation. After the run, the reference state is subtracted to each image, then smoothing and gray level normalization are used to enhance the image contrast.[17–19] By measuring the average gray level of each image, we have a measure of the average normalized magnetization; by relating it to the external field we are able to construct the magneto-optical hysteresis loop, valid for the particular region under examination.

The MFM system was operated in tapping/lift mode with commercial MESP (Co-Cr) tips with a coercivity of ≈32 kA/m. All images have been taken at the remanence, after in-plane magnetic saturation.

MOKE and MFM complement each other, since the employed MOKE setup detects the in-plane magnetization, whereas the MFM apparatus is sensitive to magnetic poles, arising either from out-of-plane magnetic domains in materials with perpendicular anisotropy, or domain walls (especially between domains whose magnetization is not at 180° in materials with in-plane anisotropy).

Static hysteresis loops have been measured on all samples by means of a vectorial vibrating sample magnetometer (VSM) equipped with an 8-coil setup.[20] The sample can automatically rotate along the z direction, as shown in Fig. 1. This setup simultaneously acquires the components of the magnetization vector $\vec{M}$ along the direction of the applied magnetic field $\vec{H}_a$ (the x direction) and a direction orthogonal to it (y). These components of $\vec{M}$ are then called M_x and M_y, respectively. Dependent on how the sample is placed into the electromagnet gap, two configurations are possible, as represented in Fig. 1:

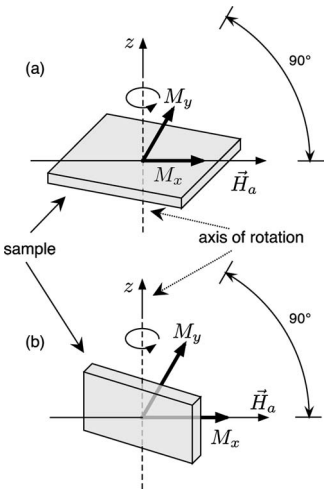

FIG. 1. Relative position of sample, axis of rotation, applied magnetic field $\vec{H}_a$, and magnetization components M_x and M_y. (a) The specimen revolves around the z axis, lying in the (x,y) plane. Thus, $\vec{H}_a$ is always applied in-plane for any sample orientation. (b) As the specimen rotates about the z axis, $\vec{H}_a$ (always directed along the x direction) is in general applied out-of-plane, making any possible angle with the film plane itself.

(a) The magnetic field $\vec{H}_a$ is applied in the film plane (x,y), where both components M_x and M_y lie too; the specimen rotates along a direction orthogonal to the film plane itself (z);

(b) the position of the film plane with respect to the applied field $\vec{H}_a$ changes; for a given angle, $\vec{H}_a$ is in the film plane and the two components of $\vec{M}$ are, respectively, in plane (M_x) and out of plane (M_y); if the specimen is 90° rotated with respect to this configuration, $\vec{H}_a$ is orthogonal to the plane and M_x (always parallel to $\vec{H}_a$) is out of plane, whereas M_y is in- plane; at any intermediate angle, both M_x and M_y do not lie in the film plane.

On each sample, a full set of static vector hysteresis loops has been measured as a function of the sample angular position, in both configurations.

III. VECTOR MODEL FOR MAGNETIZATION PROCESSES IN TWO DIMENSIONS

We will now discuss the model developed for studying the vector anhysteretic properties of our thin films. Preliminary results, presented in Ref. 9 will be summarized here, and new results will also be developed and reported. The theoretical model will then be exploited in Sec. IV to discuss the experimental results.

This approach, based on the Néel phase theory (NPT) and exploited for soft magnetic systems with uniaxial anisotropy, was at first applied to disk-shaped amorphous samples with a

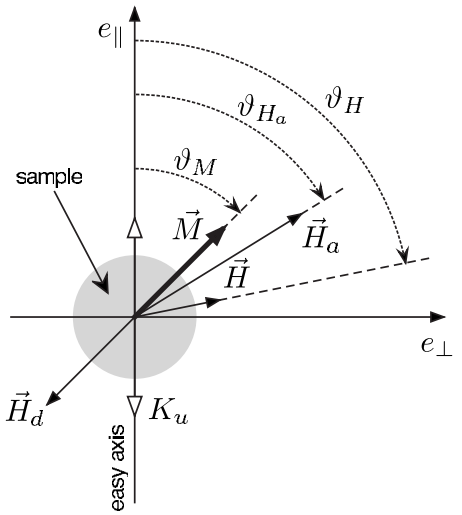

FIG. 2. Relative orientations of applied field $\vec{H}_a$, demagnetizing field $\vec{H}_d$, effective field $\vec{H}=\vec{H}_a+\vec{H}_d$, and magnetization $\vec{M}$, with respect to the easy axis of the macroscopic anisotropy (with constant K_u), induced in the sample.

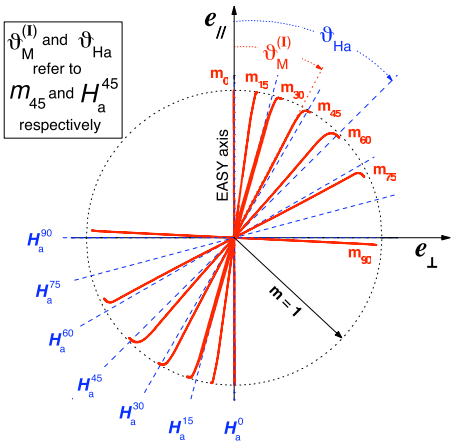

FIG. 3. (Color online) Commercial Co-based VITROVAC 6030 amorphous alloy. Evolution of the relative average magnetization $\vec{m}=\vec{M}/M_s$ [or of the loci $m_{\parallel}(m_{\perp})$] in the disk plane sample (solid curves). The applied field $\vec{H}_a$ oscillates along a fixed direction ϑ_{H_a} (dashed lines) with respect to the easy axis of the sample. Seven experimental conditions are pictured: $\vartheta_{H_a}=0°, 15°, 30°, 45°, 60°, 75°, 90°$. The angle $\vartheta_M^{(I)}$ indicates the average megnetization direction when the magnetic system lies in mode I (see text).

formerly induced macroscopic in-plane easy axis (Fig. 2), disregarding any hysteresis effects,[9] which were discussed to some extent in Refs. 10 and 11.

The specimen was assumed as magnetically homogeneous and the effect of the domain structure was neglected. Consequently, the average magnetization $\vec{M}$, the demagnetizing field $\vec{H}_d=-N_d\vec{M}$ (wherein N_d is the demagnetizing coefficient due to the sample shape), and the effective field $\vec{H}=\vec{H}_a+\vec{H}_d$ are uniform inside it. Figure 2 shows all the vector quantities in the sample plane $(e_{\parallel},e_{\perp})$, where ϑ_{Ha}, ϑ_H and ϑ_M are the angles formed by $\vec{H}_a$, $\vec{H}$ and $\vec{M}$ with the *easy axis*, respectively (notice that the angle formed by $\vec{H}_d$ is again ϑ_M).

As reported in Ref. 9 in detail, the behavior of the magnetic system can be discussed only accounting for the anisotropy, Zeeman, and demagnetizing field energy terms. In uniaxial systems, only one phase or two phases with identical energies can appear: this latter case corresponds to a set of finely spaced domains, with almost opposite magnetization. In Fig. 3, the experimental results already obtained in Ref. 9 are reported: the *loci* of the relative magnetizations $m_{\parallel}$ vs $m_{\perp}$ (wherein $m_{\parallel}=M_{\parallel}/M_s$ and $m_{\perp}=M_{\perp}/M_s$ are the relative magnetizations along the *easy* and *hard axes*, respectively) are displayed for different orientations of the applied field $\vec{H}_a$ (notice that only the particular angle $\vartheta_M=\vartheta_M^{(I)}$, corresponding to $\vartheta_{H_a}=45°$ is shown).

Two distinct regimes of the magnetization reversal are noticeable. As $\vec{H}_a$ is decreased from high and positive values, the relative average magnetization $\vec{m}=\vec{M}/M_s$ is seen to follow the circumference of radius $m\equiv|\vec{m}|=1$, rotating away from the $\vec{H}_a$ direction (which can be reached only in the limit case $H_a\to+\infty$). In this region, the coherent rotation of $\vec{m}$ reveals the presence of only one magnetic phase in the sample. This magnetization regime $(\vartheta_M^{(I)}\leq\vartheta_M<\vartheta_{H_a}$ and $M\equiv|\vec{M}|=M_s)$, called mode II if one adopts the NPT terminology, holds until the applied field gets the threshold $H_{a,lim}(\vartheta_{H_a};K_u,N_d)$ and ϑ_M correspondingly reaches its lower limit value $\vartheta_M^{(I)}$. In the range $-H_{a,\mathrm{lim}}\leq H_a\leq H_{a,\mathrm{lim}}$ it is possible to demonstrate that two magnetic phases coexist in the sample (mode I). Consequently, the magnetization direction remains constant $(\vartheta_M=\vartheta_M^{(I)})$, and m progressively decreases until the negative saturation is reached $(m=-1)$. Finally, when $H_a<-H_{a,lim}$, $\vec{m}$ again follows a symmetric curved path along the circumference (mode II).

The magnetization direction ϑ_M in mode II, when the sample is saturated $(m=1)$, can be computed by exploiting the Stoner–Wolhfarth model. Mode I is instead discussed in detail in Ref. 9, where the two master equations for the modulus and the direction of $\vec{m}$ are worked out:

$$m=\sqrt{\left(\frac{H_{a\parallel}}{H_{\mathrm{ds}}}\right)^2+\left(\frac{H_{a\perp}}{H_{\mathrm{ds}}+H_K}\right)^2} \tag{1}$$

$$\tan\vartheta_M^{(I)}=\frac{H_{\mathrm{ds}}}{H_{\mathrm{ds}}+H_K}\tan\vartheta_{H_a} \tag{2}$$

being $H_{\mathrm{ds}}=N_dM_s$, and $H_K=2K_u/(\mu_0M_s)$ the anisotropy field.

From such a background, in this paper, the model has been further developed, leading to the following results. From Eq. (1), with $m=1$, and by remembering that $H_{a\parallel}=H_a\cos\vartheta_{H_a}$ and $H_{a\perp}=H_a\sin\vartheta_{H_a}$ (with $H_a=|\vec{H}_a|$), one obtains an equation for the threshold value $H_{a,lim}$, only involving the sample parameters H_{ds} and H_K, and the given orientation of the applied field ϑ_{H_a}:

$$H_{a,\mathrm{lim}}=\left[\left(\frac{\cos\vartheta_{H_a}}{H_{\mathrm{ds}}}\right)^2+\left(\frac{\sin\vartheta_{H_a}}{H_{\mathrm{ds}}+H_K}\right)^2\right]^{-1/2}. \tag{3}$$

Moreover, from Eqs. (2) and (3) it is possible to work out two expressions connecting $H_{a,\mathrm{lim}}$ to the constant H_{ds},

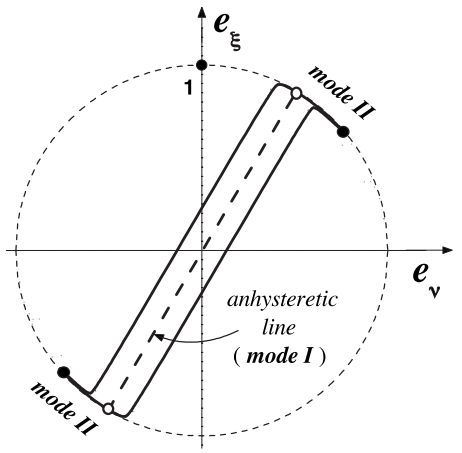

FIG. 4. Example of a $m_\xi(m_\nu)$ locus in the case that any reference direction is unknown. The locus shows an hysteretic effect which is, as a first approximation, neglected, considering an anhysteretic line. This line is assumed to represent mode I, whereas the curved paths on the circumference, between the open and full dots, correspond to mode II.

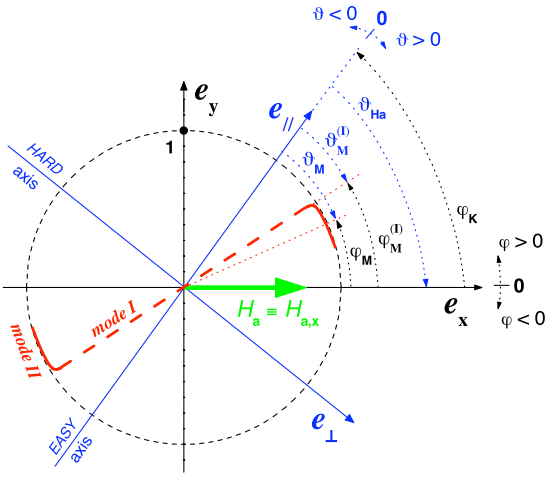

FIG. 5. (Color online) Relative position of the two reference frames $(e_\perp, e_{\|})$ and (e_x, e_y). The axes from which the angles are measured are $e_{\|}$ and e_x, respectively. From the figure, relations (6)–(8) are easily verified. Notice that positive (negative) ϑ angles are measured clockwise (counterclockwise) in the $(e_\perp, e_{\|})$ frame, whereas the opposite convention is adopted for φ angles in frame (e_x, e_y).

$$H_{\rm ds} = H_{a,\rm lim}\frac{\cos\,\vartheta_{H_a}}{\cos\,\vartheta_M^{(I)}} \tag{4}$$

and to the constant H_K,

$$H_K = H_{a,\rm lim}\left[\frac{\sin\,\vartheta_{H_a}}{\sin\,\vartheta_M^{(I)}} - \frac{\cos\,\vartheta_{H_a}}{\cos\,\vartheta_M^{(I)}}\right], \tag{5}$$

respectively.

For the Co-based VITROVAC 6030 amorphous sample investigated in Ref. 9, Eqs. (4) and (5) give $H_{ds}=267$ A/m, from which, being $J_s \equiv \mu_0 M_s = 0.82$ T, one gets $N_d = 4.1 \times 10^{-4}$ and $H_K = 275$ A/m, respectively. The obtained value of the demagnetizing coefficient is in good agreement with the theoretical one ($N_d \cong 6.2 \times 10^{-4}$ for an ellipsoid with dimensions comparable with sample size), which is computed with the usual expressions available for oblate ellipsoids (see, e.g., Ref. 21).

It is remarkable that if the orientation of the sample *easy axis* with respect to $\vec{H}_a$, and the characteristic parameters $H_{\rm ds}$ and H_K are unknown, this model can be exploited to obtain this information. The procedure is outlined below.

The starting point is an experimental $m_\xi(m_\nu)$ locus (or a set of loci), pictured in a Cartesian reference frame (e_ν, e_ξ), where the axes do not have any particular orientation with respect to the sample, but are orthogonal to one another. The first step is to neglect any presence of hysteresis, drawing an *anhysteretic line* that crosses the axes origin and plays the role of the *anhysteretic curve* (Fig. 4).

If it were possible to increase *ad libitum* the H_a value, the two tips (of mode II) of any $m_\xi(m_\nu)$ loci would define the straight line followed by the alternating applied field. A much more practicable experimental procedure is suggested from Fig. 3, where only the first and the third quadrants are involved. A first remark is that in mode II the tips always point to the $\vec{H}_a$ direction, and one can then measure the $m_\xi(m_\nu)$ loci of the sample revolved clockwise (counterclockwise) until the disappearance of mode II curve. In this way, the direction of the remaining mode I straight line, i.e., the anhysteretic line, coincides with the $\vec{H}_a$ (easy axis) direction, that is, $\vartheta_M^{(I)} = \vartheta_{H_a}$ ($\varphi_M^{(I)} = 0$). If the experimental curves lie in the second and fourth quadrants, a symmetrical procedure is followed.

At this stage, it is possible to choose the reference frame. For example, in Fig. 3 the easy axis is assumed as the the origin of the ϑ_{H_a}, ϑ_M, and $\vartheta_M^{(I)}$ angles, and the $(e_\perp, e_{\|})$ frame is then adopted. However, in the experimental setups, the $\vec{H}_a$ direction is always known, whereas the direction of the anisotropy is not, and consequently, one can assume this one (called, for example, the x direction) as the origin of the φ_K, φ_M, and $\varphi_M^{(I)}$ angles, adopting the (e_x, e_y) frame.

As displayed in Fig. 5, between these two reference frames, the following relationships hold:

$$\varphi_K = \vartheta_{H_a}, \tag{6}$$

$$\varphi_M = \varphi_K - \vartheta_M = \vartheta_{H_a} - \vartheta_M. \tag{7}$$

In particular, for mode I,

$$\varphi_M^{(I)} = \varphi_K - \vartheta_M^{(I)} = \vartheta_{H_a} - \vartheta_M^{(I)}. \tag{8}$$

Once the direction of the applied field $\vec{H}_a \equiv \vec{H}_{a,x}$ is known, only two measurements [i.e., only two $m_y(m_x)$ loci], performed (1) before and (2) after a sample rotation of a known angle α (positive or negative), are sufficient to find the *easy axis* orientation, with respect to the $\vec{H}_a$ direction, and the specimen parameters $H_{\rm ds}$ and H_K as well. In fact, by remembering the relationships (6) and (8), we can write a system for the two $m_y(m_x)$ curves (1) and (2), by exploiting the master Eq. (2):

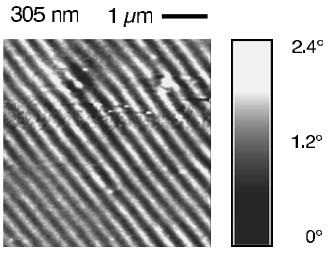

FIG. 6. MFM image of film n7 (305 nm thick) acquired using phase detection.

$$\tan[\varphi_K(1) - \varphi_M^{(I)}(1)] = h \tan \varphi_K(1) \tag{9}$$

$$\tan[\varphi_K(2) - \varphi_M^{(I)}(2)] = h \tan \varphi_K(2), \tag{10}$$

with $h = H_{\rm ds}/(H_{\rm ds} - H_K)$. Since

$$\varphi_K(2) = \varphi_K(1) + \alpha \tag{11}$$

and eliminating h from the system of Eqs. (9) and (10), we end with the following expression (independent of the values of $H_{\rm ds}$ and H_K):

$$\frac{\tan[\varphi_K(1) - \varphi_M^{(I)}(1)]}{\tan \varphi_K(1)} = \frac{\tan[\varphi_K(1) + \alpha - \varphi_M^{(I)}(2)]}{\tan[\varphi_K(1) + \alpha]} \tag{12}$$

that gives the orientation of the easy axis, for the sample in position "1:" $\varphi_K(1)$, being the quantities $\varphi_M^{(I)}(1)$ and $\varphi_M^{(I)}(2)$ both known from experiments.

One must remark that Eq. (12) is valid only when both loci lie in the first and second quadrants. If instead they occupy the second and fourth quadrants, the more convenient approach is to tip the curves over the x axis (due to the the fact that in this calculation we consider mode I only, we simply have to change the sign of the $\varphi_M^{(I)}$ angles), and then change the sign of α and of the obtained value φ_M. When more complicated situations arise, it is possible to work out a formula very similar to Eq. (12), accounting for the periodicity of the trigonometric functions.

Finally, after measuring the $H_{a,\rm lim}$ value (for the specimen in position "1"), corresponding to the threshold between mode I and mode II in the $m_y(m_x)$ locus, and thanks again to relations (6) and (8), Eqs. (4) and (5) give the values of $H_{\rm ds}$ and H_K, respectively.

The demagnetizing coefficient $N_d = H_{ds}/M_s$ (and thus, the demagnetizing field $\vec{H}_d = -N_d\vec{M}$) and the anisotropy constant $K_u = \frac{1}{2}\mu_0 M_s H_K$ are consequently obtained.

IV. RESULTS AND DISCUSSION

A. Film n7 (305 nm thick): K_u out of plane

Film n7 is characterized by an uniaxial magnetic anisotropy, with *easy axis* orthogonal to the film plane (with constant K_u), as clearly evidenced by MFM images, sensitive to the field component perpendicular to the film plane, that reveal a remanence state (after previous in-plane saturation) constituted by a stripe domain configuration (Fig. 6). It has to be remarked that MFM detects only *surface* magnetization; as a consequence, the observed stripe domain configuration may not be representative of the whole sample thickness. Nothing is known from MFM concerning the domain pattern inside the sample volume, and, as we will see in the following paragraphs, there are indications that whereas the surface of film n7 is perpendicularly magnetized, some of its volume may be magnetized in the plane. In addition, the stripe domain configuration detected by MFM may not be due to a magnetization perfectly aligned with the perpendicular anisotropy axis, but may be due to an oscillating magnetization vector with an in-plane component and an out-of-plane component that periodically changes sign.[8]

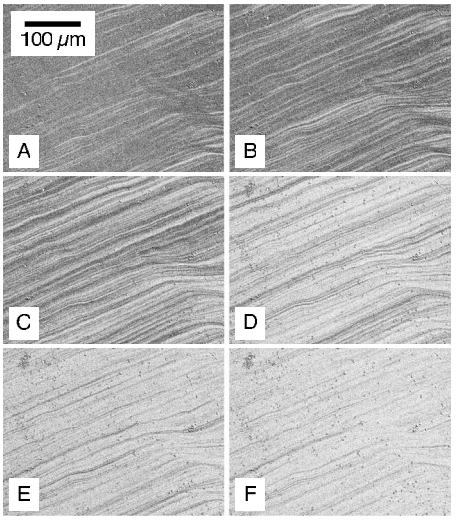

FIG. 7. MOKE images of sample n7 (305 nm thick) corresponding to field values of (a) 1909, (b) 2144, (c) 2370, (d) 2598, (e) 2815, and (f) 3034 A/m. The field is applied in the horizontal direction. The scale length shown in (a) is 100 μm.

MOKE images, taken at a few selected applied magnetic fields, are shown in Fig. 7 and are an example of *dense stripe domain* structure, where a huge number of very thin stripes run parallel to the applied field. This observation is in agreement with what was already discussed concerning the MFM image on the same sample (see Fig. 6). However, MFM and MOKE alone cannot provide a thorough description of the magnetic domain configuration over the whole sample volume.

For this reason, hysteresis loops and magnetic anisotropy have been studied by means of the vectorial VSM setup which was described above. The two experimental conditions described at the end of Sec. II [Figs. 1(a) and 1(b)] are now investigated for film n7.

1. Applied field $\vec{H}_a$ in plane

This case is shown in Fig. 8, where the uniaxial anisotropy, with constant K_u, displays an *easy axis* along the z direction (axis of rotation).

Figure 9 reports the measured $m_y(m_x)$ locus (wherein $m_y = M_y/M_s$ and $m_x = M_x/M_s$ are the relative magnetizations along the y and x axes, respectively) for a generic direction of the sample with respect to the applied field $\vec{H}_a \equiv \vec{H}_{a,x}$. Independent of the specimen orientation, all the $m_y(m_x)$ curves are always superimposed and almost aligned along

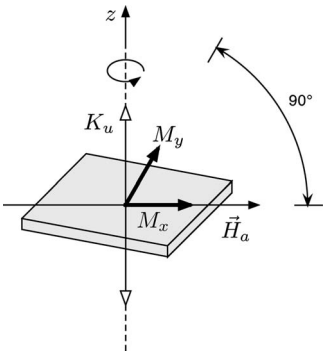

FIG. 8. Measurement configuration for film n7, when $\vec{H}_a$ is applied in the sample plane. Note the presence of an easy axis (with constant K_u) perpendicular to the film plane.

the x direction. This result establishes that shape anisotropy is negligible (when the field is applied on the film plane), and the uniaxial in-plane anisotropy detected by MOKE images is too small to be detectable by means of VSM measurements.

In Fig. 9, hysteresis is not noticeable. Whereas adopting the more conventional representation, shown in Fig. 10 for a generic direction of the sample, a $m_x(H_{a,x})$ hysteresis loop appears (with coercive field $H_c \approx 2700$ A/m). The dense stripe domain structure discussed in Figs. 6 and 7 is associated with a typical (see, e.g., Refs. 13 and 22–24) two-step behavior of the hysteresis loop of film n7: coming from saturation, in correspondence to the anisotropy field H_K associated with the perpendicular anisotropy, the rotation of the magnetization from in-plane saturation to the out-of-plane configuration occurs, thus determining an almost linear contribution to the M_x vs H_a curve. At a field $H_{a,w}$ (of opposite sign with respect to the initial saturation), a steep switching behavior occurs, marking a large in-plane magnetization reversal process. The switching process occurring at $H_{a,w}$ accounts for almost half of the saturation magnetization of film n7. This switching may involve the dense stripe domains observed by MOKE (see Fig. 7) and MFM (see Fig. 6), with the magnetization vector having both in-plane and out- of-plane components,[8] or some deeper domains, magnetized in the plane: detailed studies of the hysteretic processes occurring in these films are thus required (mostly anhysteretic processes are discussed in this paper) to clarify this point.

The anisotropy field can be estimated as the field at which rotations start to appear, coming from saturation. In this

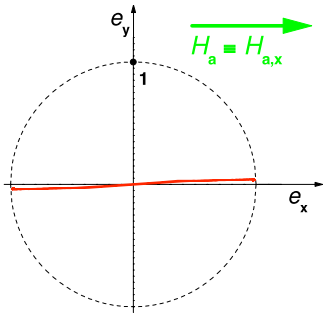

FIG. 9. (Color online) $m_y(m_x)$ locus of film n7 for a generic orientation of the applied field (in plane) with respect to the sample.

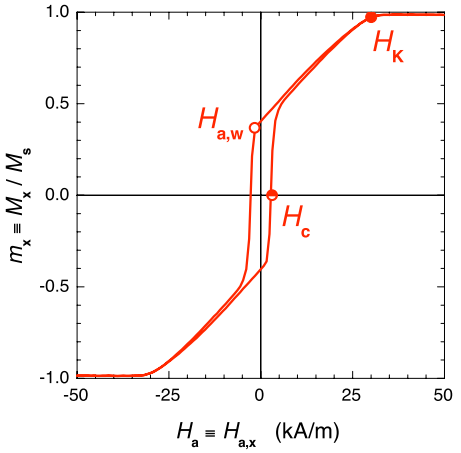

FIG. 10. (Color online) $m_x(H_{a,x})$ hysteresis loop of film n7, with the field applied in plane, along a generic direction with respect to the specimen orientation.

way, one obtains $H_K \approx 32$ kA/m and a corresponding anisotropy constant $K_u = \frac{1}{2}\mu_0 M_s H_K \approx 23$ kJ/m^3 by assuming $J_s \equiv \mu_0 M_s = 1.45$ T. This is the value of the out-of-plane anisotropy, which is responsible for the dense stripe domains observed by MFM (see Fig. 6) and MOKE (see Fig. 7), and for the magnetization rotation between $H_{a,w}$ and H_K. The obtained value of the anisotropy constant is worth a few comments; the quality factor $Q = K_u/K_d$ is usually considered a good estimate of the capability of a material to display perpendicular magnetization (see, e.g., Refs. 13 and 25), where $K_d = \frac{1}{2}\mu_0 M_s^2 \approx 8.4 \times 10^5$ J/m^3 ($M_s \approx 1.15 \times 10^6$ A/m or $\mu_0 M_s \approx 1.45$ T is assumed as the saturation value for the studied alloy). When $Q > 1$, a spontaneous perpendicular magnetization is assumed, both in the single-domain and multidomain state. However, even values of Q that are lower than 1 (*weak stripe domain* condition) are compatible with the development of a stripe domain configuration (at the magnetic remanence) if the film thickness overcomes a threshold equal to $t_{cr} = 2\pi\sqrt{A/K_u}$. In our case, the perpendicular anisotropy value is known from the hysteresis loops ($K_u \approx 23$ kJ/m^3), whereas the stiffness constant A is not. However, in amorphous alloys, A usually lies in the interval $(1-2) \times 10^{-11}$ J/m that gives a threshold value

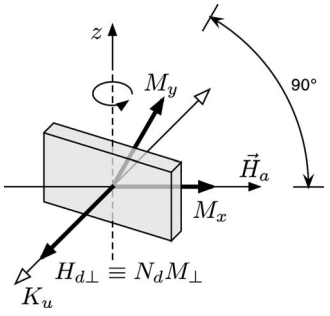

FIG. 11. Measurement configuration for film n7, when $\vec{H}_a$ is in general applied in an out-of-plane direction. Note the presence of an easy axis (with constant K_u) perpendicular to the film plane. The only non-negligible component of the demagnetizing field is oriented perpendicular to the film plane ($H_{d\perp}$).

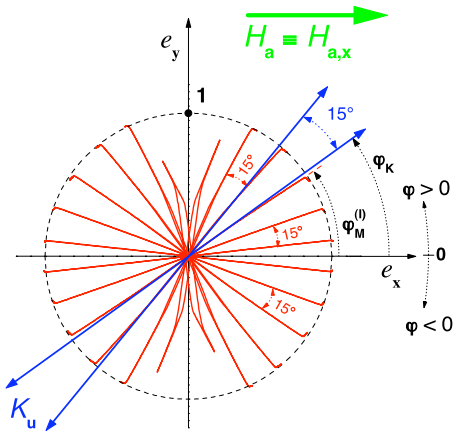

FIG. 12. (Color online) Evolution of the $m_y(m_x)$ loci of film n7 (solid lines). The applied field $\vec{H}_a$ oscillates along the x direction. Twelve different orientations of the sample are considered. The figure displays all the corresponding $m_y(m_x)$ loci but only two anisotropy axes for the sake of clarity.

$t_{cr} \approx 130-190$ nm. Film n7 is thicker than this threshold and is therefore compatible with the development of a stripe domain configuration even with a quality factor value $Q \approx 3 \cdot 10^{-2}$, much lower than 1. Under these conditions, and at zero applied magnetic field, the stripe domain width w should be comparable to the threshold thickness $w \approx t_{cr}$.[13] With reference to Fig. 6, a stripe average width $w = 177 \pm 15$ nm is obtained, which is in good agreement with the t_{cr} previously estimated.

2. Applied field H_a out of plane

The geometry is now switched to that of Fig. 1(b) (as displayed in detail in Fig. 11), and selected experimental $m_y(m_x)$ loci are depicted in Fig. 12. The orientation of the curves with respect to the applied field will be discussed in the following paragraphs. In order to discuss these results, we are now assisted by the model described in Sec. III,[9–11] where, at first stage, hysteresis effects are neglected. This approach was originally developed to describe the evolution of $\vec{M}$ lying in the sample plane $(e_\parallel, e_\perp)$, where also $\vec{H}_a$ was applied and the easy axis was contained (see Fig. 2). In that case, $\vec{H}_d$, due to shape anisotropy, was almost uniform throughout the disk- shaped sample, easily measurable, and a quite accurate appraisal of its value was also possible. The model, however, is still valid if $\vec{M}$, $\vec{H}_a$, and $\vec{H}_d$ and the easy axis belong to the same plane, which can also be not coincident with the sample surface. This condition is fulfilled in the experimental conditions now examined, where the above mentioned physical quantities lie in the (e_x, e_y) plane (see Figs. 11 and 12). The in-plane demagnetizing field due to specimen geometry is negligible, as demonstrated in Sec. I; as a consequence, the demagnetizing coefficient N_d along the out-of-plane direction is ≈ 1, and the only non-vanishing component of the demagnetizing field is $H_{d\perp} \equiv N_d M_\perp$.

In the measurements performed by means of the VSM setup, the orientation of the specimen with respect to the $\vec{H}_a$ direction is unknown, which is contrary to the rotation angle of the sample between two next measurements: $\alpha = 15°$. However, as already observed for Fig. 3, the tips of the $m_y(m_x)$ curves always point toward the $\vec{H}_a$ direction, and the $m_y(m_x)$ loci assume the shape of straight lines when the applied field direction coincides with the easy axis. It is then easy to obtain a figure like Fig. 12 by simply rotating the axes in order to obtain $m_y(m_x)$ loci symmetrically placed on the two sides of the x direction. In this way, the direction of the applied field $\vec{H}_a \equiv \vec{H}_{a,x}$ with respect to the specimen orientation becomes known.

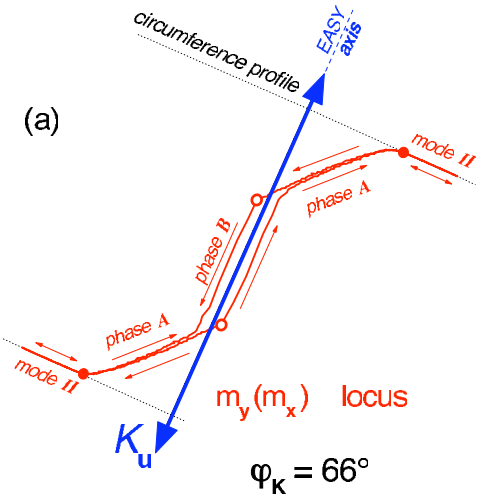

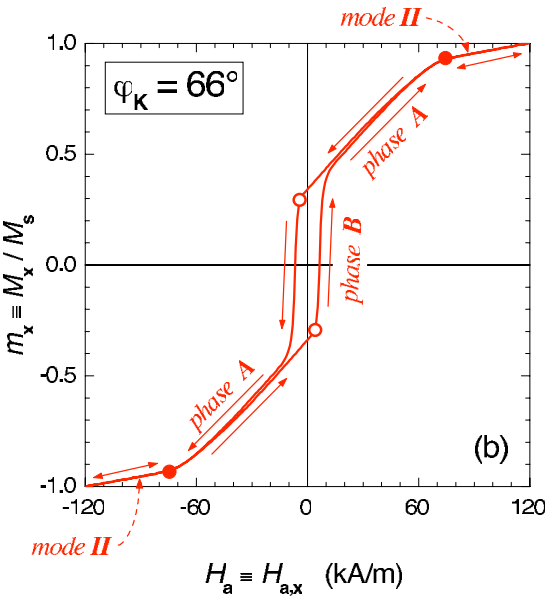

FIG. 13. (Color online) Film n7, with the sample rotated at an angle $\varphi_K = 66°$, with respect to the applied field direction (similar behaviors are found for $\varphi_K \neq 66°$). (a) Enlargement along a direction perpendicular to the easy axis of the locus $m_y(m_x)$; (b) $m_x(H_{a,x})$ hysteresis loop. In both (a) and (b), the different *phases* are shown. The points corresponding to the threshold value $|H_{a,\mathrm{lim}}|$ ($|H_{a,w}|$) are represented by full (open) dots. The continuous arrows indicate the path followed by the average relative magnetization $\vec{m}$ (or $m_x(H_a)$), as a consequence of the alternating applied field $\vec{H}_a \equiv \vec{H}_{a,x}$.

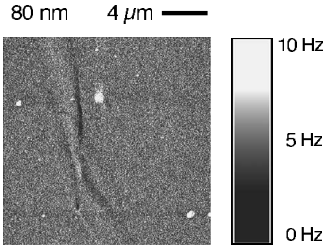

FIG. 14. MFM image of film n8 (80 nm thick) acquired using frequency shift.

By means of the procedure outlined in Sec. III [Eqs. (9)–(12)], which is iterated for any couple of loci, the angle formed with $\vec{H}_{a,x}$ by the sample easy axis, for any orientation of the specimen, is worked out. Being the induced anisotropy bound to the sample, its position is also known. Figure 12 displays the experimental $m_y(m_x)$ loci, together with the orientation of uniaxial anisotropy (only two easy axes are drawn, for the sake of clarity). The figure points out the fact that the $m_y(m_x)$ curves are almost superimposed to the easy axis direction, with mode II portion very less pronounced. This behavior is in agreement with the pretty high value of K_u estimated in Sec. I.

It is also possible to get this result by observing (from Fig. 12) that any locus can be obtained (at least for medium-low polarization values) by simply revolving the adjacent one by an angle $\alpha=15°$: the same rotation angle of the sample. In other words,

$$\varphi_M^{(I)}(2) = \varphi_M^{(I)}(1) + \alpha \tag{13}$$

and Eq. (12) then becomes

$$\frac{\tan[\varphi_K(1) - \varphi_M^{(I)}(1)]}{\tan\,\varphi_K(1)} = \frac{\tan[\varphi_K(1) - \varphi_M^{(I)}(1)]}{\tan[\varphi_K(1) + \alpha]}, \tag{14}$$

which gives (apart from the trivial case $\alpha=0$)

$$\varphi_K(1) = \varphi_M(1) \quad \text{or} \quad \vartheta_M^{(I)} = 0, \tag{15}$$

Furthermore, a shortcut to this conclusion can also be worked out without invoking the model equations. Being the uniaxial anisotropy direction bound to the sample (perpendicular to its surface in this case), the angular difference between two adjacent easy axes must be $\alpha=15°$, that is, $\varphi_K(2)=\varphi_K(1)+\alpha$, indeed. This fact, together with the loci properties remarked by Eq. (13), brings to the conclusion that for symmetry reasons mode I of any locus must be coincident with the corresponding easy axis direction. The two $m_y(m_x)$ loci closest to the y axis correspond to a situation where the maximum applied field is not sufficient to bring to the circumference limit the $m_y(m_x)$ loci. Furthermore, Fig. 12 shows that these are the only cases wherein hysteresis is noticeable, in this representation.

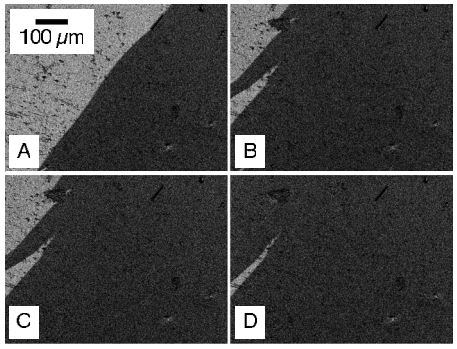

FIG. 15. MOKE images of film n8 (80 nm thick) corresponding to field values of (a) 172, (b) 180, (c) 204, and (d) 208 A/m. The field is applied in the horizontal direction. The scale length shown in (a) is 100 μm.

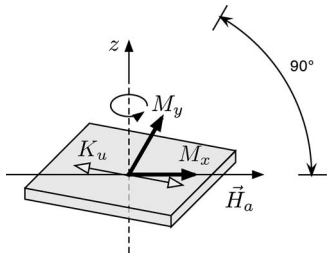

FIG. 16. Measurement configuration for film n8, when $\vec{H}_a$ is applied in the sample plane. Note the presence of an easy axis (with constant K_u) in the film plane itself.

In these experimental conditions, the real magnetization process is much more complicated than the ideal one postulated in the framework of the model outlined in Sec. III. The straightforward application of such an approach can thus give only a rough description of the real magnetization inversion, which involves different kinds of domains. Consequently, the usual description of magnetization inversion involving the so-called mode I must be dropped.

To give a deeper insight into these phenomena, it is useful to draw artificial enlargements of the $m_y(m_x)$ loci, perpendicularly to the associated easy axis, discussing in parallel the corresponding $m_x(H_{a,x})$ hysteresis loop. An example of such a procedure is given in Fig. 13, for the $\varphi_K=66°$ case.

In mode II, pure rotation brings the magnetization vector to align to the applied field $\vec{H}$. At a field $H_{a,lim}$ (full dots in Fig. 13), a nucleation of a closure domain pattern occurs,[25] leading to an intermediate phase A that persists until $H_a=H_{a,w}$ (open circles in Fig. 13), where a terminology similar to the one of Sec. I is employed. Here, irreversible processes dominate the magnetization reversal (phase B). A full understanding of the domains configuration responsible for the observed hysteretic behavior and for the values of $H_{a,w}$ is not yet available and is beyond the scope of this paper.

B. Film n8 (80 nm thick): K_u in plane

Film n8 is characterized by an in-plane magnetic anisotropy (with constant K_u), as MFM (Fig. 14) and MOKE (Fig. 15) clearly point out. The MFM image (taken at the remanence after previous in-plane saturation) reveals no magnetic contrast, indicating a magnetization mostly lying in the film plane (no significant z components of the magnetic field generated by the surface magnetization are detected); a defect on the surface of the sample pins the magnetization, and faint halos propagate from the defect, revealing a charged domain

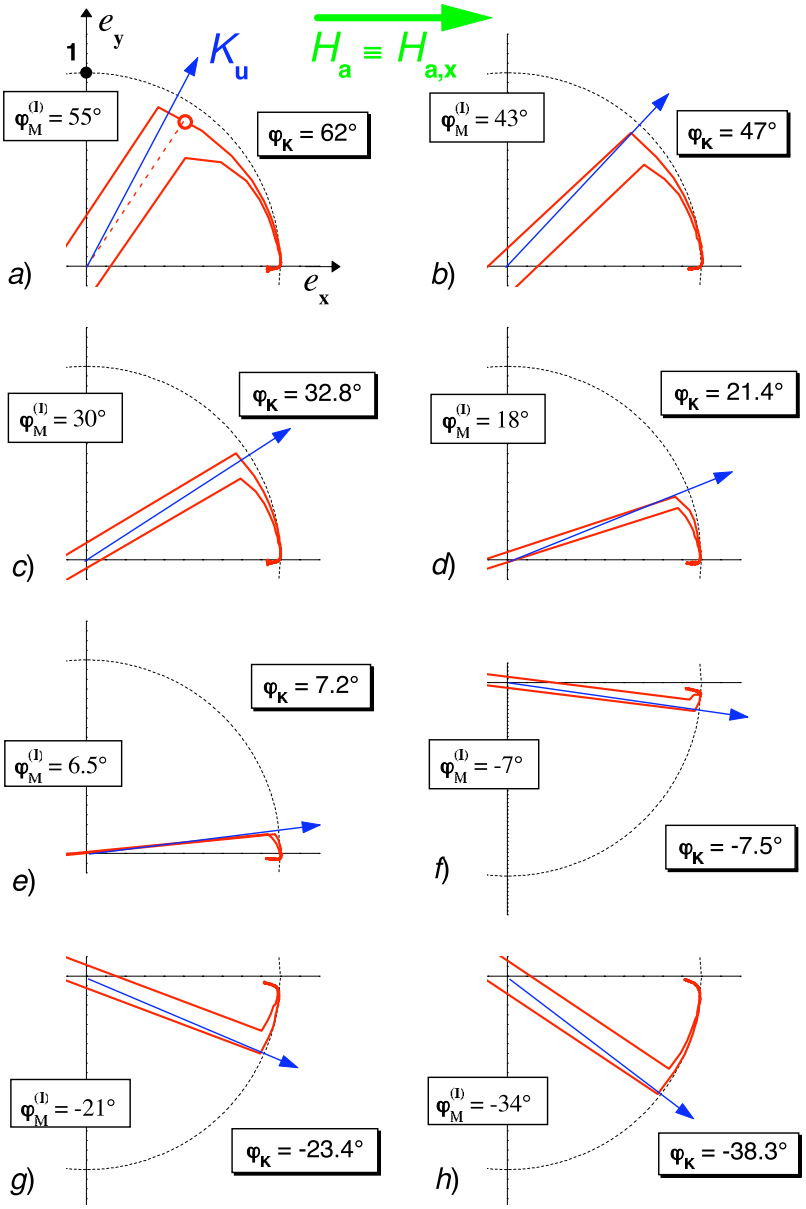

FIG. 17. (Color online) Behavior in the first quadrant of eight selected $m_y(m_x)$ loci of film n8 (solid lines) for different sample orientations. The arrows represent the in-plane uniaxial anisotropy with constant K_u. The applied field $\vec{H}_a$ oscillates along the x direction. In all cases, the $\varphi_M^{(I)}$ measured angle, formed by the anhysteretic line [depicted only in (a) for the sake of clarity] with $\vec{H}_x \equiv \vec{H}_{a,x}$ is shown. The open dot at the crossing point between the anhysteretic line and the locus is assumed to correspond to the $H_{a,lim}$ value. The φ_K angles are calculated from the model by means of Eq. (12), with $\alpha = 15°$.

wall between magnetic domains with in-plane magnetization. MOKE detects large magnetic domains with walls that suddenly move causing a quick magnetization reversal.

1. Applied field $\vec{H}_a$ in plane

By means of the vectorial VSM setup, hysteresis and magnetic anisotropy have been investigated on film n8, in the configuration described in Fig. 1(a) (as shown in detail in Fig. 16).

Thirteen measurements of the $m_y(m_x)$ loci, with a different orientation of the sample with respect to $\vec{H}_a \equiv \vec{H}_{a,x}$, were performed, and eight of them are shown in Fig. 17 (see Fig. 5 for angles meaning).

The very same procedure outlined in Sec. IVA2 allowed us to correctly orient these curves with respect to the applied field direction, after neglecting the hysteresis effects, considering in their place the so-called *anhysteretic line* (mode I). Iterative application of Eq. (12), being $\varphi_M^{(I)}$ known from the figure and the sample rotated by $\alpha = 15°$ after each measurement, gave the calculated position of the easy axis (i.e., of the film plane) φ_K. The computed angular differences between two successive measurements are listed in Table I. We found $|\Delta\varphi_K| \cong \alpha$ in all cases, a result which demonstrates the consistency of the adopted procedure.

The $H_{a,\mathrm{lim}}$ value is now obtained from the crossing point between the anhysteretic line and the corresponding $m_y(m_x)$ locus (an example is given in Fig. 17(a)). We found $\langle H_{a,\mathrm{lim}} \rangle \cong 400$ A/m (see Fig. 18) and, by remembering Eqs. (6) and (8), the relationships 4 and 5 give $\langle H_{\mathrm{ds}} \rangle \cong 330$ A/m, and $\langle H_K \rangle \cong 3500$ A/m, respectively. Therefore, one ends with the following in-plane demagnetizing constant $\langle N_d \rangle \cong 2.86 \times 10^{-4}$, which is in fairly good agreement with the one calculated in Ref. 26 ($\approx 1 \times 10^{-4}$).

The magnitude of the uniaxial in-plane anisotropy results $K_u \cong 2500$ J/m^3: one order of magnitude lower than the value of the out-of-plane anisotropy constant (sample n7, discussed in Sec. I), which was in fact able to keep the av-

TABLE I. Referring to Fig. 18, the table reports the modulus of the angular differences $|\Delta\varphi_K|$ (calculated throughout the model) between two adjacent easy axes of the uniaxial anisotropy bound to the sample, when the latter is rotated by an angle $\alpha=15°$. The apexes refer to labels of Fig. 18.

	$\lvert\Delta\varphi_K\rvert$ (°)
$\varphi_K(a)-\varphi_K(b)$	15.0
$\varphi_K(b)-\varphi_K(c)$	14.2
$\varphi_K(c)-\varphi_K(d)$	11.4
$\varphi_K(d)-\varphi_K(e)$	14.2
$\varphi_K(e)-\varphi_K(f)$	14.7
$\varphi_K(f)-\varphi_K(g)$	15.9
$\varphi_K(g)-\varphi K(h)$	14.9

erage polarization $\vec{M}$ almost parallel to the easy axis, for a wide range of applied fields (see Fig. 12). In the present case, with respect to what was reported in Ref. 9, the origin of the uniaxial in-plane anisotropy is not to be searched in the sample shape. In fact, for the case of sample n7, we concluded that it was possible to neglect the in-plane demagnetizing field, connected with the specimen shape; since specimen n8 is much thinner, this conclusion is *a fortiori* valid. The origin of the in-plane uniaxial anisotropy and of the non-negligible N_d value is then to be ascribed to some other cause. In the case of sputtered thin films, effects acting during film deposition, like a slight tilting or bending of the substrate[27] are often invoked to account for such effects, especially when magnetostriction is not negligible.[28] In our materials, magnetostriction should be of the order of $\approx 30 \times 10^{-6}$ (Ref. 29) and can thus be the source of the in-plane anisotropy (of both films n7 and n8) if small residual stresses are assumed in the as-prepared films due, for example, to a slight bending of the substrate when kept in place by its frame in the deposition chamber.

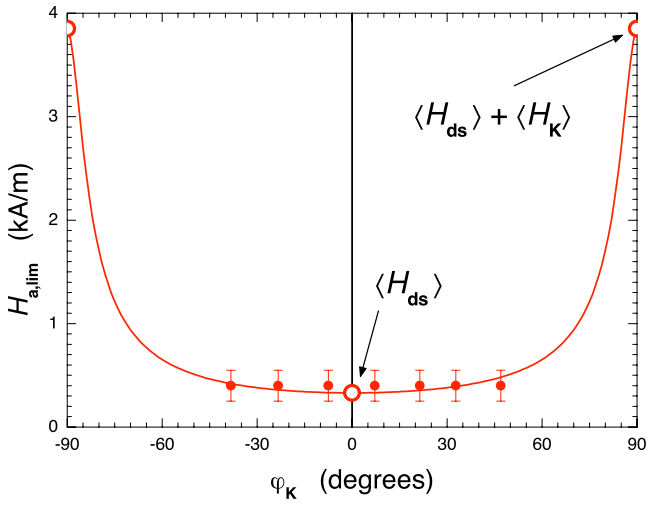

FIG. 18. (Color online) Experimental values (full dots) and theoretical behavior of $H_{a,lim}$ vs φ_K [the continuous curve is calculated from Eq. (3)] for film n8. The open dots represent the values of $\langle H_{ds}\rangle$ and $\langle H_{ds}\rangle+\langle H_K\rangle$. In the range $-50° \leq \varphi_K \leq +50°$, the quantity $H_{a,lim}$ is shown to be almost constant.

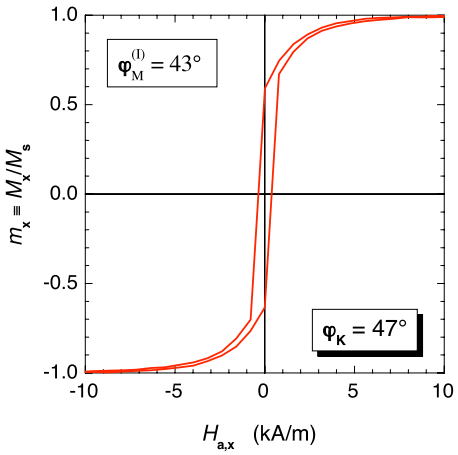

FIG. 19. (Color online) $m_x(H_{a,x})$ hysteresis loop of film n8, corresponding to the locus displayed in Fig. 17(b). The in-plane applied field makes an angle $\varphi_K=47°$ with respect to the specimen easy axis.

Finally, from the knowledge of H_{ds} and H_K, we can draw [Eq. (3)] the theoretical behavior of $H_{a,\mathrm{lim}}$ vs φ_K, as shown in Fig. 18. This curve is in agreement with the almost constant experimental $H_{a,\mathrm{lim}}$ values found, for a wide range of φ_K around zero, which is a further confirmation of the consistency of the approach.

Comparing Fig. 12 to Fig. 17, one remarks that the hysteresis effects are much more pronounced in the film n8. An example, adopting the more conventional representation of hysteresis, is given in Fig. 19. It corresponds to the $m_x(m_y)$ locus of Fig. 17(b). Compared to Fig. 10, Fig. 19 clearly shows the disappearance of the two-phase magnetization process, with a softer magnetic behavior and an approach to saturation described by a curved, almost reversible loop shape, which could be ascribed to the presence of in-plane closure domains and rotation of the magnetization off the direction of the in-plane magnetic anisotropy.

V. CONCLUSIONS

The magnetization process of ferromagnetic materials has an intrinsic vector nature, but both from the theoretical and experimental point of view, most efforts deal only with scalar properties, and a general theory of vector magnetization processes is still lacking. Magnetic anisotropies play a key role in determining how the average magnetization vector changes as a function of the applied magnetic field or of sample shape, through coherent and/or incoherent rotations of the local magnetization and domain wall assisted magnetization reversals.

In this paper, the magnetization process has been studied in two FeSiB amorphous thin films that display either uniaxial out-of-plane or in-plane magnetic anisotropy, depending on their thickness. The availability of a single ferromagnetic material with macroscopically different magnetization processes, when prepared in identical conditions except for the thickness, is particularly helpful for studying

the vector magnetization processes both experimentally and theoretically. To this aim, a vector model has been described and extended, and its results have been applied to the experimental data in order to understand the contribution of sample shape and magnetic anisotropy. While sample shape has been proven to be important only when the magnetization vector has an out-of- plane component, the role of other magnetic anisotropies has been shown both theoretically and experimentally to strongly influence the magnetization processes of the studied ferromagnetic thin films.

[1] P. Ripka, *Magnetic Sensors and Magnetometers* (Artech House, Norwood, MA, 2001).

[2] S. Khizroev and D. Litvinov, *Perpendicular Magnetic Recording* (Kluwer, Dordrecht, 2004).

[3] E. Della Torre, Physica B (Amsterdam) **343**, 1 (2004).

[4] H. Pfützner, PTB bericht E-81 (Braunschweig, 2003), pp. 81–87.

[5] Y. Yoshida, M. Enokizono, T. Todaka, and G. Shirakawa, J. Magn. Magn. Mater. **196-197**, 904 (1999).

[6] G. Radley and A. Moses, IEEE Trans. Magn. **MAG-17**, 1311 (1981).

[7] Z. Y. Liu and S. Adenwalla, Phys. Rev. B **67**, 184423 (2003).

[8] A. Asenjo, D. García, J. M. García, C. Prados, and M. Vázquez, Phys. Rev. B **62**, 6538 (2000).

[9] C. Appino and V. Basso, Physica B (Amsterdam) **343**, 39 (2004).

[10] C. Appino, J. Magn. Magn. Mater. **290-291**, 471 (2005).

[11] C. Appino and M. Coïsson, Physica B (Amsterdam) **372**, 133 (2006).

[12] M. Coïsson, F. Celegato, E. Olivetti, P. Tiberto, F. Vinai, and M. Baricco (to be published 2008).

[13] A. Hubert and R. Schäfer, *Magnetic Domains* (Springer-Verlag, Berlin, 1998).

[14] B. Argyle and J. McCord, in *Efficient Kerr Microscopy*, NATO Science Series II: Mathematics, Physics, and Chemistry, edited by G. C. Hadjipanayis, (Springer, 2001), Vol. 41, pp. 287–305.

[15] B. Argyle, *Magneto-Optic Microscope System for Magnetic Domain Studies*, Proceedings of the Symposium on Magnetic Materials, Processes and Devices, edited by L. T. Romankiw and D. A. Herman, Jr. (The Electrochemical Society, Pennington, N.J., 1990), Vol. 90-8, pp. 85–109.

[16] S. Defoug, R. Kaczmarek, and W. Rave, J. Appl. Phys. **79**, 6036 (1996).

[17] F. Schmidt, W. Rave, and A. Hubert, IEEE Trans. Magn. **21**, 1596 (1985).

[18] F. Laviano, R. Gerbaldo, G. Ghigo, L. Gozzelino, G. Lopardo, B. Minetti, and E. Mezzetti, Physica B **403**, 293 (2008).

[19] M. Nixon and A. Aguado, *Feature Extraction and Image Processing* (Elsevier Science, New York, 2002).

[20] J. P. C. Bernards, Rev. Sci. Instrum. **64**, 1918 (1993).

[21] F. Fiorillo, *Measurement and Characterization of Magnetic Materials*, Elsevier Series in Electromagnetism, edited by I. Mayergoyz (Elsevier, New York, 2004).

[22] P. Sharma, H. Kimura, A. Inoue, E. Arenholz, and J. H. Guo, Phys. Rev. B **73**, 052401 (2006).

[23] J. Yu, C. H. Chang, D. Karns, G. P. Ju, Y. Kubota, W. Eppler, C. Brucker, and D. Weller, J. Appl. Phys. **91**, 8357 (2002).

[24] *Handbook of Thin Film Technology*, edited by L. I. Maissel and R. Glang (McGraw-Hill, New York, 1983).

[25] M. Ghidini, G. Zangari, I. L. Prejbeanu, G. Pattanaik, L. D. Buda-Prejbeanu, G. Asti, C. Pernechele, and M. Solzi, J. Appl. Phys. **100**, 103911 (2006).

[26] A. Aharoni, J. Appl. Phys. **83**, 3432 (1998).

[27] M. Vázquez, D. García, C. Prados, A. Asenjo, F. J. Castaño, K. Mandal, J. M. García, M. Tena, and A. Hernando, IEEE Trans. Magn. **36**, 3968 (2000).

[28] R. Krishnan, M. Tessier, M. C. Contreras, and I. Iglesias, IEEE Trans. Magn. **28**, 2427 (1992).

[29] P. Allia and F. Vinai, Phys. Rev. B **26**, 6141 (1982).